Interplay of plasma-induced and fast thermal nonlinearities in a GaAs-based photonic crystal nanocavity

Alfredo de Rossi,* Michele Lauritano,† Sylvain Combrié, Quynh Vy Tran, and Chad Husko‡
Thales Research and Technology, Route Départementale 128, 91767 Palaiseau, France
(Received 28 April 2008; revised manuscript received 6 October 2008; published 16 April 2009)

We investigate the nonlinear response of GaAs-based photonic crystal cavities at time scales which are much faster than the typical thermal relaxation rate in photonic devices. We demonstrate a strong interplay between thermally and carrier-induced nonlinear effects. We have introduced a dynamical model entailing two thermal relaxation constants which is in very good agreement with experiments. These results will be very important for photonic crystal-based nonlinear devices intended to deal with practical high repetition rate optical signals.

DOI: 10.1103/PhysRevA.79.043818 PACS number(s): 42.70.Qs, 42.65.Pc

I. INTRODUCTION

With both a small modal volume and large quality factor, optical microcavities exhibit a greatly enhanced light-matter interaction and a strong nonlinear optical response [1–4]. An emerging class of optical microcavities is based on air-clad two-dimensional (2D) photonic crystals (PCs). A Q factor of greater than 10^6 was achieved with this technology [5–7] which also allows small modal volumes [$\approx(\lambda/n)^3$ or 10^{-19} m^3]. Moreover, 2DPC technology is a planar technology which is particularly suited for the fabrication of photonic circuits. Therefore, the move toward all-optical processing, long considered impractical, has changed dramatically and new possibilities have been opened [8]. Impressive experimental demonstrations of low-energy (fJ) optical bistability and all-optical switching [9–11], wavelength conversion [12], optomechanical effects [13], and dynamical control of the cavity lifetime [14] are recent noteworthy achievements. Most of these results come from a specific technology, i.e., silicon-based air-clad PCs where the nonlinear process involved is two-photon absorption (TPA) followed by plasma-induced and thermally induced refractive index changes. The optical power required is quite small ($\approx$100 fJ) and can be very fast (70 ps by ion implant, as the carrier recombination time result is much shorter in these nanostructured devices than in bulk silicon [15,16]. It has been predicted that, owing to strong light-matter interaction, nonlinear properties can be engineered by introducing nanoparticles [17].

The desire for an even faster response time motivates the research on alternative materials with a strong optical Kerr effect. Much progress has been made in processing chalcogenide crystals with high-Q PC microcavities, which have been demonstrated recently [18]. III-V semiconductors are also good candidates for optical switching as they have two very attractive features, compared with silicon. First, the optimization of the Kerr effect with respect to TPA [19,20]. Self-phase modulation due to Kerr effect has been demonstrated in 2DPCs recently [21,22]. An additional feature of III-V semiconductors is the possibility of exploiting a strong nonlinear effect related to absorption saturation in active structures, such as quantum wells (QWs) and quantum dots (QDs). Fast nonlinear dynamics [23], leading to bistability [24] and excitability [25], has been observed in InP-based 2DPCs with InAsP QWs which are designed to operate with band-edge modes coupled to off-plane free-space beams. Low power and very fast (2 ps) switching (15 ps for a complete on-off cycle) has been demonstrated with a symmetric Mach-Zehnder-type all-optical switch made with InAs/AlGaAs quantum dots [26].

In this paper we focus on the dynamics of the processes initiated by TPA in GaAs PCs. Although, ideally, all optical switching requires the Kerr effect, in practice TPA, followed by a carrier-induced index change, is still a very attractive approach because of the relative simplicity of the technology. In particular, there is no active material, e.g., QDs, or phase matching condition required. Moreover, compared to silicon, the TPA coefficient in GaAs is tenfold higher [27] and the nonradiative carrier lifetime in patterned structures can be very short (8 ps) [28]. A fast and strong nonlinear response is therefore expected in GaAs PC nanocavities. Very recently, we have demonstrated ultrafast (6 ps recovery time) and low-power ($\approx$150 fJ) modulation in GaAs photonic crystal cavities [29]. We have investigated optical bistability in high-Q ($Q=0.7\times10^6$) PC cavities on GaAs and reported an ultralow threshold power (μW range) [30–32]. Recently, memory operation has been demonstrated in a InGaAsP PC cavity [33].

In these experiments, only the slow (μs) regime has been explored, which is dominated by the thermally induced index change. This is also due to the high thermal resistance of the membrane structures compared to, for instance, microdisks [34] or membranes bonded to a SiO_2 cladding [24] and the lower thermal conductivity of GaAs with respect to silicon.

In this paper we investigate the response of PC microcavities at a much faster modulation rate (up to 50 MHz), which is well beyond the typical thermal relaxation time of photonic devices. Under these conditions, the analysis of nonlinear responses, such as bistability, cannot be explained with static models. First of all, moving to faster time scales modifies the relative influence of thermal and carrier plasma effects. While at very fast time scales (ps) the dynamics tend to be controlled by the carrier lifetime, we will show that in the range of 1–100 ns the dynamics results from the interplay of

*alfredo.derossi@thalesgroup.com
†Also at Department of Engineering, University of Ferrara, Italy.
‡Also at Columbia University, New York, USA.

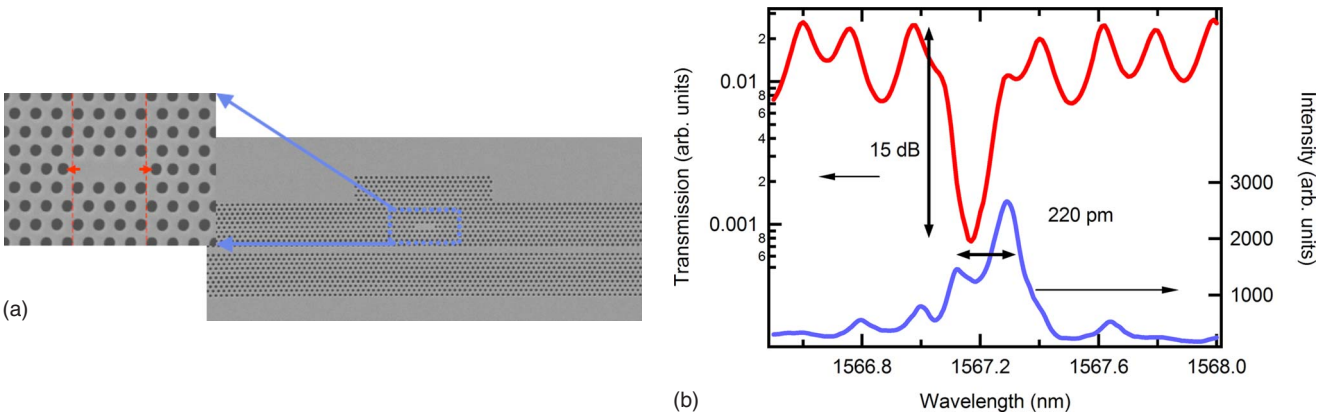

FIG. 1. (Color online) (a) Scanning electron micrograph (SEM) image of the sample, also showing a line-defect photonic crystal waveguide with side coupled *L*3 cavity. (b) Linear transmission near resonance showing that the cavity is overcoupled. The linewidth of the cavity is larger than the transmission dip because of interplay with the Fabry-Pérot fringes. The left scale is the waveguide transmission and the right scale is the signal detected by the ir camera.

fast thermal effects and carrier plasma index shift. We present a model that incorporates two thermal relaxation constants. This is necessary to explain this dynamics and the fact that, despite the high thermal resistance of PC microcavities, there are thermal effects which develop in less than 10 ns. Section II is devoted to experiments made on a PC microcavity coupled to a waveguide. In Sec. III we will present our multiscale model. Discussion of the results forms the body of Sec. IV.

II. EXPERIMENTAL SETUP AND SAMPLE DESCRIPTION

The photonic crystal structure studied here is the well-known optimized three missing holes (*L*3) PC microcavity [35] in an air slab structure (thickness is 265 nm) based on a triangular lattice (period $a=400$ nm) of holes with radius $r=0.24a$. The holes at the cavity edge were shifted by $s=0.15a$. The cavity is side coupled (the spacing is three rows) to a 1-mm-long line-defect waveguide along the ΓK direction, with width $W=1.05\sqrt{3}a$ (see Fig. 1). The fabrication process and the detailed linear characterization of similar structures are described elsewhere [36]. The loaded and intrinsic Q factors, 7000 and 30 000, respectively, are estimated from measurements using the procedure discussed in a previous paper [37]. The cavity resonant wavelength is 1567 nm. The characterization setup consists of a tunable external cavity semiconductor laser (Tunics) with a relative accuracy of 1 pm and narrow linewidth ($\ll 1$ MHz), which is amplified by an erbium-doped fiber amplifier (EDFA). The polarization is set to TE, or electric field in the plane of the slab. Coupling to the PC waveguide is obtained through microscope objectives [Zeiss, numerical aperture (NA)=0.95] and micropositioners. The transmitted signal is detected with an InGaAs photodiode (bandwidth=2 GHz), amplified (40 dB, transimpedance and 2 GHz bandwidth), and monitored by an oscilloscope (Tektronix, 12.5 GS/s).

Two distinct regimes of modulation are considered: (1) sinusoidal modulation (frequency from few kHz to 50 MHz) and (2) low duty cycle (20 ns) square pulses. The cavity is observed from the top with a microscope (long working distance objective Zeiss, NA=0.4) and an infrared InGaAs camera (Xenics). When the cavity is on resonance a bright spot is observed.

A. Sinusoidal modulation

At a low modulation rate (kHz) it has been shown by several groups [9–11,31,32] that bistability occurs at a fairly low optical power (μW range, coupled into the waveguide). The dominant nonlinear effect is thermally induced index change because of heating resulting from carriers generated by TPA. Since this effect leads to a redshift of the cavity frequency, bistability is observed when the initial detuning $\Delta\lambda|_{t=0}=\lambda_{\text{laser}}-\lambda_{\text{cavity}}|_{t=0}$ is positive, where $\lambda_{\text{cavity}}|_{t=0}$ is the cold cavity resonant wavelength. This is shown in Fig. 2. Typically, the detuning is set between $\sqrt{3}/2$ (the theoretical minimum, although it has been shown that the Fabry-Pérot resonances in the waveguide affect this value [11]) and several times the cavity linewidth, estimated to be $\Delta\lambda_{\text{FWHM}}=220$ pm in our case. If the modulation frequency is increased while the detuning and the average signal power are kept constant, the bistable behavior disappears. For instance, with a detuning $\delta\lambda\approx 330$ pm$\approx 1.5\Delta\lambda_{\text{FWHM}}$ and a modulation frequency of 15 kHz, bistability is observed in this sample at 80 μW. The power coupled into the waveguide is estimated considering the amplified laser power and the input objective coupling factor (here ~ -10 dB) as in our previous work [31].

When the modulation frequency is increased to 1 MHz, the bistable effect and all traces of nonlinear distortion of the transmitted signal disappear. This could be explained in terms of the slow response of the thermo-optical effect. An important question arises whether the carrier plasma effect, much faster but weaker, will then take over. To answer that, the signal power and the modulation frequency were increased further and the detuning (still positive) was swept continuously from zero to about +700 pm, with the laser always on. This detuning value is larger than in low-frequency experiments. A strong nonlinear distortion of the transmitted signal is then observed. The onset of the nonlin-

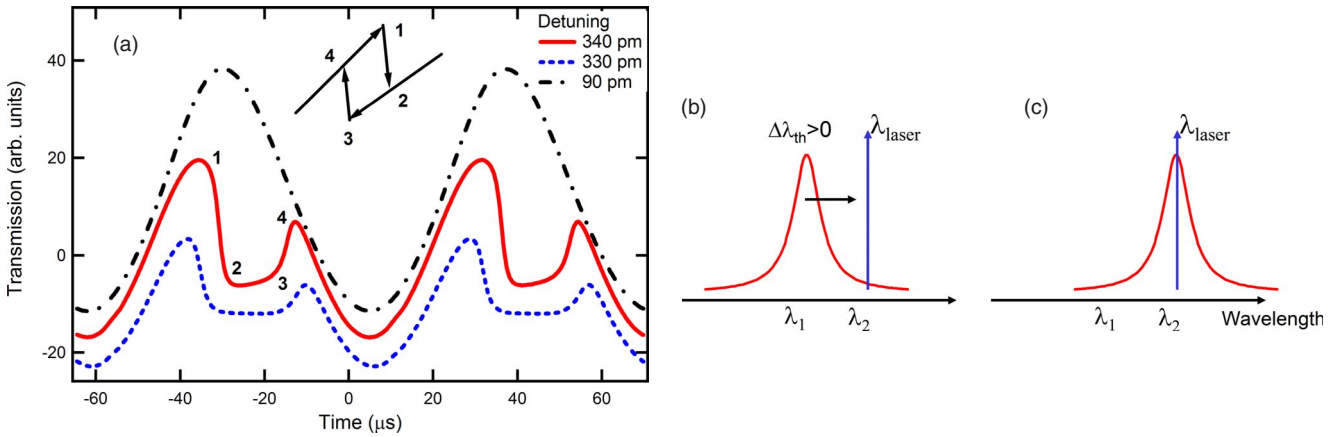

FIG. 2. (Color online) Low modulation frequency experiment. (a) Oscilloscope traces showing the typical bistable response of a PC microcavity at low modulation frequency (15 kHz). The average input power in the PC waveguide is about 80 μW. The bistable cycle is also sketched and the transitions 1–4 are also marked. Detunings are +0.4, +1.5, and +1.55$\Delta\lambda_{FWHM}$, respectively. Scheme representing a cavity with a (b) negative detuning and (c) going to resonance due to nonlinearly induced redshift.

ear behavior is simultaneous to the observation of a bright spot through the infrared camera, thus indicating that the resonant frequency of the cavity is redshifted under a sinusoidal modulation pump. In particular, Fig. 3 shows a typical output signal when the modulation frequency is increased to 50 MHz and the average power coupled in the waveguide is about 2.5 mW. The thermo-optic effect, driving the bistability at low modulation frequency, integrates over time. This explains ultralow power levels. At higher modulation frequencies the power required to observe nonlinear effects increases. The nonlinear behavior is observed with a positive detuning from 600 and 670 pm ($\approx 3\Delta\lambda_{FWHM}$). We do not believe that the observed nonlinear distortion corresponds to a bistable behavior. Indeed, a fast nonlinear mechanism (plasma-induced index change) should dominate all other nonlinearities. That is probably not the case, as the short lifetime of carriers in GaAs compared to silicon drastically reduces the strength of this effect, compared to thermo-optic effects.

The nonlinear distortion observed in Fig. 3 is quite general and can be reproduced at different modulation frequencies in the 10–100 MHz range. The nonlinear transitions are not sharp, compared to the modulation period (response time is a few ns). This time is however much faster than what could be attributed to a thermal effect. Additionally, the period, $T=20$ ns, is much shorter than what is estimated to be the thermal recovery time in air slab PC cavities [9]. We claim that the faster carrier plasma effect plays a key role at the ns time scale, while the thermal effect accumulates to strongly redshift the cavity.

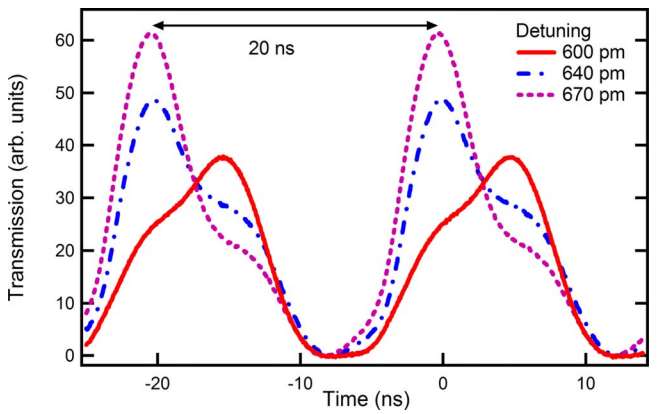

FIG. 3. (Color online) High modulation frequency experiment: oscilloscope traces of the transmitted signal with sinusoidal modulation (50 MHz) for different detunings. The average power is about 2.5 mW.

This mechanism is represented in Fig. 4. Initially, (a) the cavity is at room temperature and laser is detuned negatively ($\Delta\lambda<0$). (b) The laser wavelength is increased continuously. The cavity is blueshifted (plasma effect) very fast, but heating quickly dominates and keeps the cavity redshifted until the end of the modulation cycle. Therefore, the cavity will be pushed toward longer wavelengths as long as the heat generated by TPA over each cycle compensates the thermal flow across the membrane. (c) Over each modulation cycle, the cavity resonant wavelength will oscillate about an equilibrium point set by this thermal balance alternating blueshift and fast heating. The strongest distortion of the sinusoidal modulation is observed nearest to the largest detuning which can be sustained. In our case, we achieved detunings of up to 700 pm, which is related to a local temperature increase of 6 K through the thermo-optical coefficient (Table I). Better physical insight into the two competing effects (thermal and free carrier) is gained by reducing the average input power, e.g., considering much smaller duty cycles.

B. Low duty cycle excitation

The cavity is excited with low duty cycle square pulses (duration $\Delta t=20$ ns and period $T=2$ μs), so that the cavity has time to cool down before the arrival of the next pulse. We refer to this case as a "nonheating pulse" because the average temperature of the cavity remains close to room temperature. Figure 5 reports the input and the transmitted pulses depending on various wavelength detunings. The input power in the pulse is estimated to be on the order of 10 mW. A more accurate determination of this value was com-

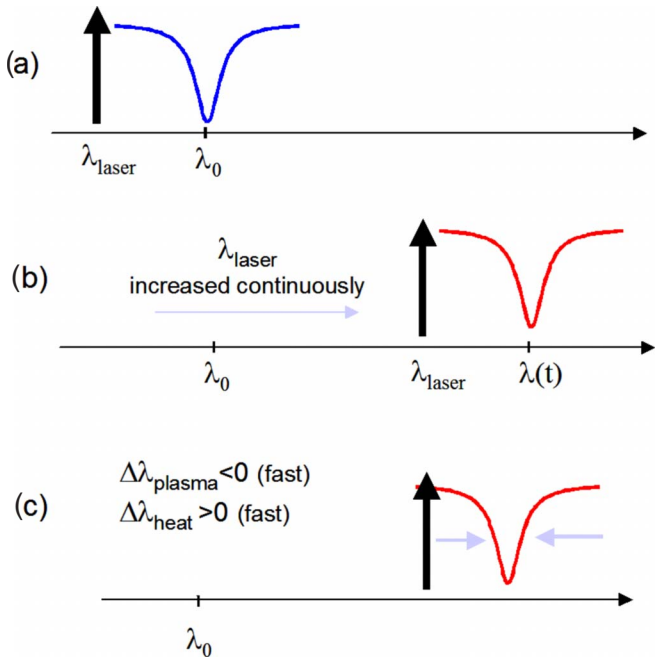

FIG. 4. (Color online) Scheme representing the interplay of thermal and carrier plasma effects and how they are related to the detuning. (a) The system is at rest (cavity at its cold frequency) and the laser is switched on. (b) The laser wavelength is increased but heating keeps the cavity red detuned. (c) When the cavity temperature is high enough, the mean resonant wavelength gets closer to the laser and the nonlinear distortion is apparent.

plicated by the very low filling factor and the use of the EDFA, which is not designed to operate in these conditions. This lead to some fluctuations in the level of the amplified pulse. Furthermore, very low duty cycle means that the

TABLE I. Physical paramenters used in the dynamical model.

Parameter	Symbol	Value	Ref.
TPA coefficient	β_2 (cm/GW)	10.2	[27]
Kerr coefficient	n_{2I} (cm^2/W)	1.6×10^{-13}	[27]
Loaded Q	Q	7000	Meas.
Intrinsic Q	Q_0	30000	Est.
Modal volume	V_{mod}	$0.66(\lambda/n_0)^3$	Calc.
TPA volume	V_{TPA}	$3.13(\lambda/n_0)^3$	Calc.
Carrier volume	V_{car}	$7V_{\mathrm{mod}}$	
Thermo-optic coeff.	dn/dT (K^{-1})	2.48×10^{-4}	[38]
Therm. eff. vol. (c)	$V_{\mathrm{th},c}$	$3.8V_{\mathrm{mod}}$	Calc.
Therm. eff. vol. (m)	$V_{\mathrm{th},m}$	$31V_{\mathrm{mod}}$	Calc.
Specific heat	$c_v\rho$ (W/K m^{-3})	1.84×10^6	[38]
Carrier lifetime	τ_N	8 ps	[28,29]
Therm. relax. time (c)	$\tau_{\mathrm{th},c}$	8.5 ns	Calc.
Therm. relax. time (m)	$\tau_{\mathrm{th},m}$	200 ns	Calc.
Therm. resistance	$R_{\mathrm{th}}=\sum\frac{\tau_{\mathrm{th}}}{C_{\mathrm{th}}}$	7.5×10^4 K/W	Calc.
FCA cross section	$\sigma_{e,h}$ (10^{-22} m^2)	$9.3(\frac{\lambda}{1.0\ \mu\mathrm{m}})^{2.3}$	[39]

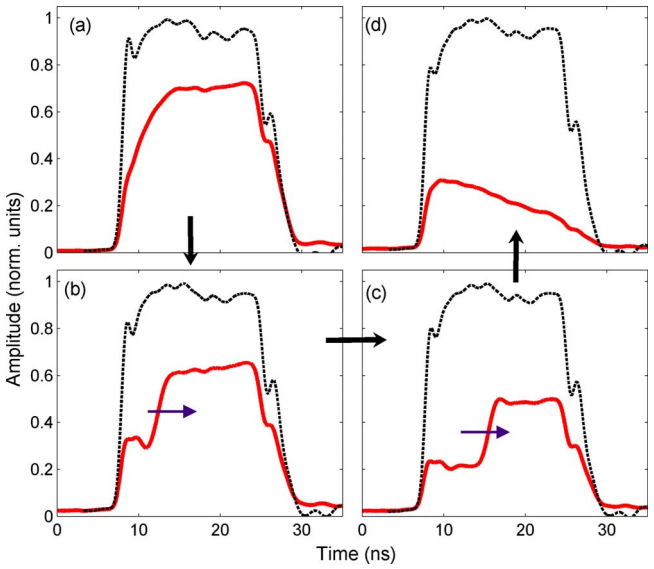

FIG. 5. (Color online) Experiment with nonheating pulses. Input (dashed line) and output (solid line) pulses as a function of the detuning. (a) $\Delta\lambda=-0.5\Delta\lambda_{\mathrm{FWHM}}$, (b) $+0.7\Delta\lambda_{\mathrm{FWHM}}$, (c) $+0.9\Delta\lambda_{\mathrm{FWHM}}$, and (d) $+1.5\Delta\lambda_{\mathrm{FWHM}}$. The pulse period is 2 μs.

power contained in the pulse is a fraction of the amplified spontaneous emission (ASE), which means that it is difficult to determine the exact value of the measurement of the average power. Let us first consider a negative detuning, e.g., $\Delta\lambda\approx-0.5\Delta\lambda_{\mathrm{FWHM}}$ [Fig. 5(a)]. The leading edge of the output pulse rises with almost linear slope and is about 5 ns long. For zero or moderate positive detuning (e.g., $\Delta\lambda$ between 0 and $\approx\Delta\lambda_{\mathrm{FWHM}}$), the output pulse typically has a two-step shape with the leading part of the pulse having a lower level [Figs. 5(b) and 5(c)]. The transition between the two levels is sharp (a few ns) and moves from the leading edge to the trailing edge of the pulse as the detuning is increased. If detuning is increased further, the pulse takes on an almost triangular shape with a sharp leading edge and a long trailing edge [Fig. 5(d)] before losing any signature of nonlinear distortion.

Interestingly, the initial leading edge of the output pulse is very similar in the four cases considered in Fig. 5, i.e., we do not see low transmittance associated to the on-resonance case, as long as the power is high. We see this behavior at much lower power only. We believe that this is due to a fast carrier effect which detunes the cavity faster than that our detection apparatus is able to measure (1 ns).

It is also important to note that no signature of a plasma-induced bistable state is observed when the detuning is negative. We think that this is because of fast heating, which dominates the plasma effect before the pulse is extinguished. These features are well explained by our model.

III. NONLINEAR DYNAMICAL MODEL

The coupled-mode model developed here is based on previous optical microcavity literature. Particular structures that have been investigated include microdisks [40] and photonic crystal cavities [41–43]. The dynamical variables are the op-

tical energy inside the cavity $|a(t)|^2$, the free-carrier density $N(t)$, and the cavity and membrane temperature $T(t)$. The model considers a single-mode [44] cavity (resonance is at ω_0 and unloaded quality factor Q_0), which is side coupled to a waveguide (the loaded Q factor is Q). The modulation of the transmission observed in Fig. 1 is related to the Fabry-Pérot resonance due to the finite reflectivity at the waveguide end facets. This spatially extended resonance has no impact on the nonlinear response (other than merely modulating spectrally the coupling into the cavity) since the associated field intensity is orders of magnitude smaller than in the cavity. The field in the cavity follows the equation

$$\frac{\partial a(t)}{\partial t} = \left(i\omega - i\omega_L - \frac{\Gamma_{\text{tot}}}{2} \right) a(t) + \sqrt{\frac{\Gamma_c}{2} P_{\text{in}}(t)}, \tag{1}$$

where ω_L is the laser frequency, $\Gamma_c = \omega_0(Q^{-1} - Q_0^{-1})$ gives the cavity to waveguide coupling strength, Γ_{tot} is the inverse (instantaneous) cavity lifetime, $P_{\text{in}}(t)$ is the power in the waveguide, and $\omega = \omega_0 + \Delta\omega_{\text{NL}}$ is the instantaneous cavity frequency. Following [41,42], the nonlinear change in the cavity frequency is given by

$$\Delta\omega_{\text{NL}} = -\frac{\omega}{n_{\text{eff}}}\Delta n = -\frac{\omega}{n_{\text{eff}}}\left[\frac{n_{2I}c}{nV_{\text{Kerr}}}|a(t)|^2 \frac{dn}{dT}\Delta T(t) + \frac{dn}{dN}N(t) \right]. \tag{2}$$

Here n is the refractive index of the bulk material and n_{eff} is the effective refractive index in the cavity, i.e., $n_{\text{eff}}^2 = \int n(\vec{r})^2 |E(\vec{r})|^2 dV / \int |E(\vec{r})|^2 dV$, and n_{2I} is the Kerr coefficient and V_{Kerr} is the Kerr nonlinear volume defined as

$$V_{\text{Kerr}}^{-1} = \frac{\int n_{2I}(\vec{r})/n_{2I} |E(\vec{r})|^4 n(\vec{r})^4 dV}{\left[\int n(\vec{r})^2 |E(\vec{r})|^2 dV \right]^2}. \tag{3}$$

The refractive index change due to the plasma effect is $dn/dN = -\omega_p^2/2n\omega^2 N$ with $\omega_p^2 = e^2 N/\epsilon_0 m^*$ as the plasma frequency. In principle, holes and electrons both contribute to this effect; however, given the much smaller effective mass of electrons in GaAs, the contribution of holes is negligible. The inverse instantaneous photon lifetime is

$$\Gamma_{\text{tot}} = \frac{\omega_0}{Q} + \Gamma_{\text{TPA}} + \Gamma_{\text{FCA}}. \tag{4}$$

The first term is the inverse linear cavity lifetime, Γ_{TPA} and Γ_{FCA} are the contributions from TPA and free-carrier absorption (FCA), respectively. The TPA term is $\Gamma_{\text{TPA}} = \beta_2 c^2/n^2 |a(t)|^2 / V_{\text{TPA}}$ with β_2 representing the TPA coefficient in units of m/W and $V_{\text{TPA}} = V_{\text{Kerr}}$ representing the nonlinear effective volume [42], while the free-carrier absorption is proportional to the combined free-carrier density $\Gamma_{\text{FCA}} = (\sigma_e + \sigma_h) N(t) c/n$. The evolution of carrier density follows the rate equation

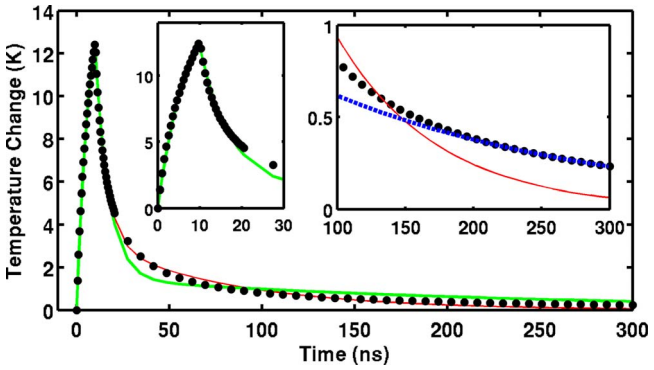

FIG. 6. (Color online) Modeling heat diffusion in the PC membrane. Local cavity temperature T_c vs time calculated with a 2D thermal diffusion equation (dots) and fitting (solid thick and thin lines) with model (6). Inset: enlarged view of the short- and the long-term behaviors. Inset right: fitted $\tau_{\text{th},m} = 200$ ns with a single exponential (dashed line). Fit with four unconstrained parameters (thin line). Constrained fit with $\tau_{\text{th},m} = 200$ ns and $\tau_{\text{th},c} = 8.4$ ns (thick solid line, main plot and left inset). Thermal capacitances for the cavity and the membrane are 0.43×10^{-12} and 3.4×10^{-12} W/K, respectively.

$$\frac{\partial N(t)}{\partial t} = -\frac{N(t)}{\tau_N} + \frac{c^2/n^2\beta_2}{V_{\text{TPA}}} \frac{1}{2\hbar\omega} \frac{1}{V_{\text{car}}} |a|^4. \tag{5}$$

Here $\hbar$ is the reduced Planck's constant, τ_N is the effective carrier lifetime, and V_{car} is the volume in which the carriers spread and recombine [42]. In this approximation, the population decay is dominated by recombination at the surface due to the large surface-to-volume ratio typical of photonic crystal structures. Carriers are assumed to spread and distribute homogeneously within the carrier volume V_{car}, which is assumed to correspond to the region of the membrane delimited by the holes around the cavity. This approximation is rough, but it is a reasonable choice.

Because of the high thermal resistance in membrane PCs, thermal effects are very important and must be modeled appropriately. This is, for instance, the scope of Ref. [45]. In contrast with existing literature, we present a more complicated model for the thermal response. We assume that the heat generated in the cavity has not yet diffused to the border of the membrane at the time scale of interest (1 ns). Therefore, a very important physical quantity is the thermal capacitance of the cavity $C_{\text{th},c} = c_v \rho V_{\text{th},c}$, associated with a small region of the membrane, with volume $V_{\text{th},c}$ roughly corresponding to the cavity volume. Heating and the spreading of the heat are modeled by solving the two-dimensional heat diffusion equation. The heat is generated for some time (10 ns) inside the cavity and then the system is allowed to cool down. We assume that the radiative and convective contributions are negligible; therefore, since the membrane is suspended in air, all the heat has to flow through it. The result of this calculation is shown in Fig. 6. The cavity temperature T_c increases with a rate that is governed by $C_{\text{th},c}$ and T_c decreases at two exponential time scales. The fast time scale $\tau_{\text{th},c}$ is associated to a relatively fast transfer of heat from the cavity, where it is generated, to the neighboring region in the

membrane. We associate a second thermal capacitance $C_{\mathrm{th},m}$ to the whole membrane. The second time scale $\tau_{\mathrm{th},m}$ takes into account the spreading of the heat over the rest of the membrane (with temperature T_m) to the bulk semiconductor structure. This picture is substantially different from previous models with a single time constant $\tau=C_{\mathrm{th},c}R_{\mathrm{th}}$ that is obtained from the thermal resistance R_{th} defined as $W=R_{\mathrm{th}}\Delta T$ (ratio between the increase in the temperature and the heating power at steady state). We will show that these two time scales play a crucial role in understanding the system response under sinusoidal and single-pulse excitations. The corresponding model entails therefore two auxiliary equations:

$$\frac{\partial T_c(t)}{\partial t} = -\frac{T_c(t)-T_m(t)}{\tau_{\mathrm{th},c}} + \frac{2\hbar\omega}{\tau_N}\frac{V_{\mathrm{car}}}{C_{\mathrm{th},c}V_{\mathrm{th}}}N(t), \tag{6}$$

$$\frac{\partial T_m(t)}{\partial t} = -\frac{T_m(t)-T_0}{\tau_{\mathrm{th},m}} - \frac{T_1(t)-T_2}{\tau_{\mathrm{th},1}}\frac{C_{\mathrm{th},c}}{C_{\mathrm{th},m}}. \tag{7}$$

The thermal effective volume of the cavity and of the membrane $V_{\mathrm{th},c}$ and $V_{\mathrm{th},m}$ and their thermal relaxation times $\tau_{\mathrm{th},c}$ and $\tau_{\mathrm{th},m}$ are obtained by fitting the solution of the heat diffusion equation with the solution of the two time constants model [Eq. (6)]. If we fit all four parameters (two time constants and two capacitances) the fit turns out to be very good in the first 50 ns, yet tends to underestimate the long time constant and therefore to underestimate the total thermal resistance. To prevent this, we first fit a simple exponential to the long-term behavior, which gives a time constant of approximately 200 ns. Then we fit the complete curve by constraining $\tau_{\mathrm{th},m}=200$ ns. The result is shown in Fig. 6 and confirms that this model is well adapted to describe the thermal behavior of PC microcavities. The result of this calculation is given in Table I.

IV. DISCUSSION

Simulations have been carried out with parameters given in Table I. All of them are well known or can be calculated or measured with reasonable accuracy. The carrier volume V_{car} is the exception. The impact of carrier diffusion has been investigated theoretically in a recent paper [46], providing some hints to explain a fast recovery time in silicon PCs. The carrier lifetime in patterned GaAs (e.g., 2DPCs) is however much shorter than in silicon. Very recently we estimated it to be about 6 ps in our GaAs cavities [29], which is consistent with previous (8 ps) estimates for GaAs PC structures [28].

In the limit where the dynamic is much slower than τ_N, which the case considered in this work, τ_N and V_{car} play the same role and what matters here is the ratio τ_N/V_{car}. To show that, let us consider the following density of the generated carriers:

$$N(t) = \frac{c^2/n^2\beta_2}{V_{\mathrm{TPA}}}\frac{1}{2\hbar\omega}\frac{\tau_N}{V_{\mathrm{car}}}|a|^4. \tag{8}$$

The blueshift of the cavity resonance due to the generated carriers is therefore proportional to the instantaneous power absorbed P_a. The redshift induced by heating is proportional to the absorbed energy and to the inverse of the thermal capacitance. Then, the relative strength of thermal and carrier effects depends on the ratio τ_N/V_{car} and on the thermal capacitance. The dynamical behavior of the system investigated here is basically determined by these two quantities.

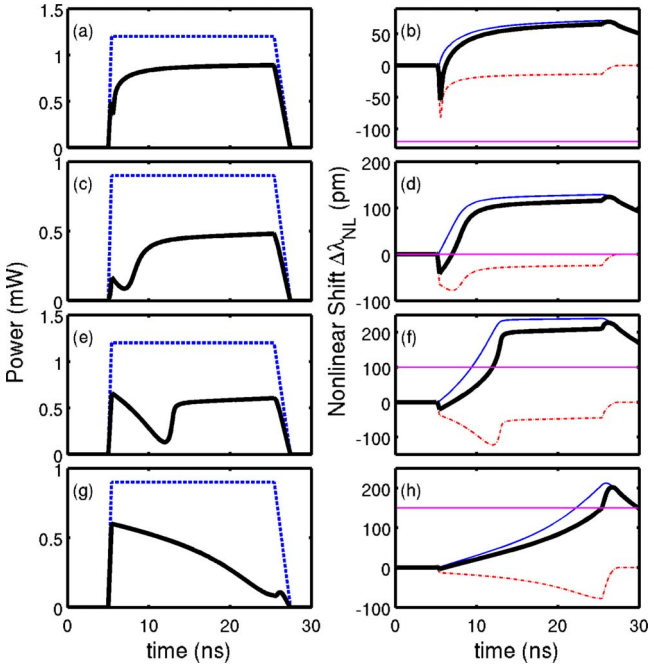

FIG. 7. (Color online) Simulation of the response (solid line) to a single pulse (dashed line), depending on the detuning $\Delta\lambda(0)$: [(a) and (b)] −120 pm, [(c) and (d)] 0 pm, [(e) and (f)] 80 pm, and [(g) and (h)] 150 pm. Right: corresponding instantaneous frequency shift $\Delta\lambda_{\mathrm{NL}}$ of the cavity resonance (solid line) and carrier plasma (thin-dashed line) and thermo-optical contributions (dotted line). The laser frequency is also shown (straight thin line). $P_{\mathrm{in}}=1.2$, 0.9, 1.2, and 1.0 mW, respectively.

Modeling was performed by varying only one parameter, the carrier volume, and adjusting the input power and the detuning around reasonable values. All other values are well known or calculated precisely.

Figure 7 reports the simulated responses of a square pulse at various detunings. When the initial detuning is negative [e.g., $\Delta\lambda(0)=-120$ pm, Figs. 7(a) and 7(b)], the carrier effect is responsible for the drop of the leading edge of the transmitted pulse. The signal coupled in the cavity is strong enough to cause considerable generation of carriers and the resulting blueshift tends to tune the cavity into resonance, so that transmission is reduced (the cavity is side coupled). Within a ns time scale, the heating following carrier recombination redshifts and therefore detunes the cavity again. Such fast heating arises from the small thermal capacitance of the cavity. After the pulse is extinguished, the cavity is redshifted by about 100 pm with respect to the initial position and recovers its initial state in a fraction of μs. Let us now consider the case of zero detuning [Figs. 7(c) and 7(d)]. The carrier-induced index change produces an instantaneous (with respect to the time scale considered here) blueshift that adds to the initial detuning. Heating, following absorption, tunes the cavity back and transmission decreases once again.

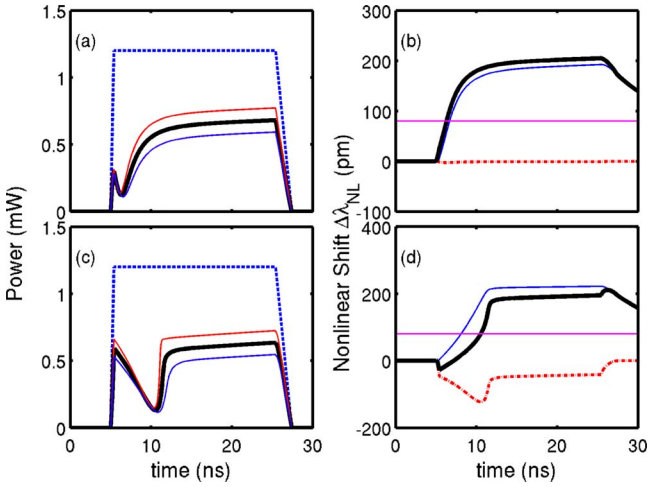

FIG. 8. (Color online) Simulated response when the contribution to the plasma shift from carrier plasma is (a) suppressed and (c) full model. The excitation power is 1.2 mW (thick line). The cases with $P_{in}=1.1$ and 1.3 mW are also plotted (thin lines). The detuning $\Delta\lambda(0)$ is 80 pm. (b) and (d) The corresponding instantaneous frequency shifts $\Delta\lambda_{NL}$ are also plotted for the case $P_{in}=1.2$ mW.

Thus more carriers are generated and the plasma effect tends to oppose heating, but in the end the heating dominates. At these modulation rates thermal relaxation is not sufficiently fast to dissipate heat from the cavity after each duty cycle. Thus heat accumulates over time, causing a net redshift of the cavity resonance. When the instantaneous detuning $\Delta\lambda_{NL}$ becomes positive, carrier generation starts to decrease and so does the carrier-induced shift. This initiates a positive feedback that quickly detunes (red) the cavity and makes the carrier density drop very fast. The delay between the pulse leading edge and this transition is clearly related to the amount of the initial detuning [Figs. 7(e) and 7(f)]. When the initial detuning is positive and large enough [Figs. 7(g) and 7(h)], then heating tends to tune the cavity into resonance, thus reducing the transmission but also generating carriers. The plasma effect will partially oppose the redshift, thus explaining an almost linear change with time. The sharp step observed in Figs. 5(b) and 5(c) can only be explained by the thermal effect overtaking the carrier plasma index change. This step cannot be reproduced for any choice of free parameters if the plasma-induced index change is suppressed in the model. This is shown in Fig. 8. In panels (a) and (b) we ran the same simulation as in Fig. 7(e), but we have suppressed the contribution of carriers to the frequency shift of the cavity. In this case the transmission increases with a linear, but finite, slope after the dip, independent of the pulse power. This is not what we see experimentally. Conversely, when the plasma effect is included, the sharp transition is reproduced correctly. There is a physical reason for that: the observed steep step requires a fast index change with, say, a negative sign and a slower index change with opposite sign. A simple explanation is that at first the plasma effect dominates (over a very short time, a few ns) before thermal heating takes over. If a plasma effect is ruled out, there is no way to explain the experimental results. A Kerr effect cannot be considered because it has the same sign as the thermal effect. Recently, critical slowing down (CSD), implying a transition from a low (off resonance) to a high (on resonance) transmission state, has been reported in InP-based PC cavities [47]. This effect also results into a step in the pulse response. We believe however that this is a different mechanism than what we describe here. The reason is that our system is side coupled; thus, CSD would manifest as a transition from a high (off resonance) to a low (on resonance) transmission state. We did not observe that. A possible explanation is the carrier lifetime in GaAs PCs being much shorter than in silicon or InP PCs. This implies that the plasma dispersion effect is much weaker than the thermally induced index change.

We found experimentally that the response of the cavity is very sensitive to the power of the pulse, in particular in the case reported in 5e. This behavior is well reproduced by theory. This means that input power must be set precisely in simulation and it cannot be the same for all the detunings considered here. Indeed, experimentally the peak pulse power is not constant since (a) the output power from the amplifier showed a marked dependence on slight change in wavelength and (b) the waveguide transmission is modulated by a strong Fabry-Pérot effect (Fig. 1). The fact that the detuning in experiments and in the theory are not the same can be understood by accepting some errors in the measurement of the detuning. The reason is that the laser was directly modulated which induced some deviations from the nominal setting of the laser on the order of 100 pm.

This relatively fast (few ns rise time) nonlinear effect reported in Fig. 5 is well understood through modeling. The complexity of the model is justified by the number of different time scales present. An important point of this paper is to demonstrate that the same model is able to explain also the response to a sinusoidal excitation. The response is calculated for a time long enough to ensure that we reach the steady-state regime. The simulations shown in Fig. 9 are carried out in order to mimic experimental conditions, that is, the excitation wavelength is detuned negatively with respect to the cold cavity frequency. As the excitation is turned on, the wavelength is increased adiabatically with respect to the modulation period. Indeed it is found that the cavity stays red detuned, and is pushed toward longer wavelengths, until the excitation power and the heat generated are enough to sustain the detuning.

The simulations clearly support the experimental results shown in Fig. 3 and interpretation in Fig. 4. Indeed, if we now compare the measured and calculated oscilloscope traces, we conclude that the dynamics are accurately reproduced, as the detunings used in modeling correspond to what is measured experimentally.

In particular, the response is very well understood by looking at the instantaneous frequency of the cavity, which crosses the laser frequency at different points depending on the detuning. If the detuning $\Delta\lambda$ is too small, the cavity wavelength is always higher than the laser frequency, as the instantaneous cavity nonlinear shift $\Delta\lambda_{NL}=\lambda_{cavity}(t)-\lambda_{cavity}(0)$ due to heating is much larger over the whole modulation cycle. When the detuning $\Delta\lambda$ increases, $\Delta\lambda_{NL}$ also increases on average, as the resonance is closer to the laser frequency, but less than $\Delta\lambda$ does. Thus,

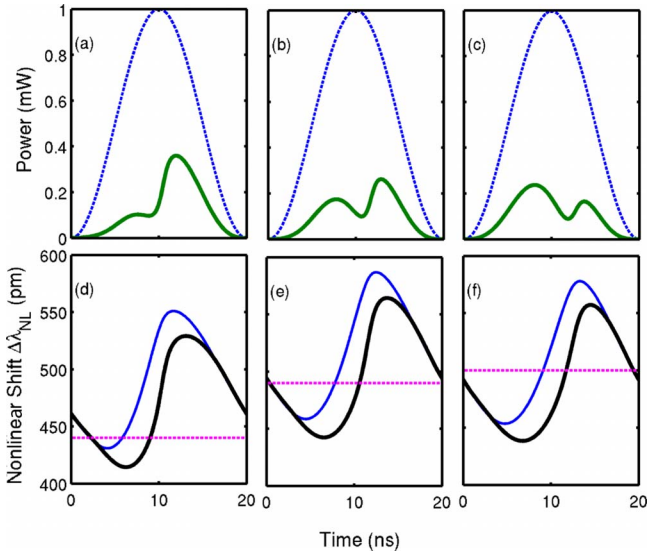

FIG. 9. (Color online) Simulation of the response of the cavity to a sinusoidal excitation for the following detunings (from top to bottom): (a) and (d) 440 pm, (b) and (e) 490 pm, and (c) and (f) 500 pm. Input peak power is 1 mW. (a)–(c) The transmitted pulses are shown on the top and (d)–(f) the instantaneous frequency shift (solid think curve) and the thermo-optical contribution alone are shown on the bottom.

there exists a combination of pulse power, modulation frequency, and detuning such that $\Delta\lambda$ and $\Delta\lambda_{NL}$ are close one to each other. If $\Delta\lambda$ is increased further, heating is not enough to keep $\Delta\lambda_{NL}$ close to it and nonlinear distortion is lost. The role of the plasma-induced index change and the interplay with the thermo-optic effect is also clear in Figs. 7(b), 7(d), and 7(f).

It is interesting to note that the plasma effect vanishes when $t<4$ ns and $t>16$ ns in Figs. 9(b), 9(d), and 9(f), although minima of the sinusoidal excitation are at $t=0$ and $t=20$ ns [Figs. 9(a), 9(c), and 9(e)]. This important point is understood when considering that while the plasma effect is almost instantaneous (within the time scale relevant to this work), the thermo-optic effect follows the time integral of the optical power. At time $t=0$ the carrier population is negligible and the cavity is cooling down and therefore is approaching the laser wavelength. As the power inside the cavity increases, carriers are generated with a rate proportional to the power squared. A carrier-induced index change builds up very fast and produces the difference between the thin and the thick curves. The power absorbed produces heating. Instantaneous heating is the time integral of instantaneous absorbed power and therefore builds up with a delay with respect to the plasma effect. The thermal effect then dominates the plasma effect. As soon as the resonance is crossed again and the detuning becomes comparable to half the cavity linewidth (100 pm), nonlinear absorption decreases very quickly and the carrier population declines accordingly. Therefore the carrier effect disappears. The cavity again starts to cool down and the cycle begins anew.

V. CONCLUSION

Switching based on TPA has a great potential in GaAs-based structures, as it benefits from the strong nonlinear absorption coefficient β_2 and sub-ns carrier lifetimes typical of this material. However, most practical applications will require a high repetition rate (i.e., high duty cycle); therefore, thermal effects are unavoidable in such small structures. In particular, heating is very strong in photonic crystals because of the poor thermal conductivity of PC membranes. We have experimentally investigated this regime and confirmed results from other groups evidencing that the thermal dynamics in PC membrane cavities is much faster than in macroscopic photonic devices due to the small modal volume of the structure. More particularly, we have explored a regime in which a sharp (2 ns) transition result from a positive feedback between thermally and carrier-induced refractive indices changes. The peak power required to see these effects is at the mW level. We have also explained why it is not possible to observe bistability in GaAs cavities when the modulation rate is on the order of 10–100 MHz. Based on these experimental results, we have presented a dynamical model for PC microcavities which includes two thermal relaxation constants in order to account for heat diffusion from the cavity to the neighboring membrane. We show that this is crucial in order to understand the dynamical response of the cavity and that this model reproduces the experimental results quite well. The ability to properly account for very different time scales is crucial for modeling patterning effects (i.e., long term or memory effects) which result not only from the carrier dynamics but also on fluctuations of the average power which induce changes in the local temperature of the cavity. This is crucial to design PC-based all-optical switches for practical optical signals at high repetition rate (e.g., 10 GHz).

ACKNOWLEDGMENT

One of the authors (C.H.) thanks the Fulbright Grant for financial support.

[1] K. J. Vahala, Nature (London) **424**, 839 (2003).
[2] V. Almeida, C. R. Barrios, R. R. Panepucci, and M. Lipson, Nature (London) **431**, 1081 (2004).
[3] M. F. Yanik and S. Fan, Phys. Rev. Lett. **92**, 083901 (2004).
[4] Q. Xu, P. Dong, and M. Lipson, Nat. Phys. **3**, 406 (2007).
[5] E. Kuramochi, M. Notomi, S. Mitsugi, A. Shinya, and T. Tanabe, Appl. Phys. Lett. **88**, 041112 (2006).
[6] B. S. Song, S. Noda, T. Asano, and Y. Akahane, Nature Mater. **4**, 207 (2005).
[7] T. Asano, B. S. Song, and S. Noda, Opt. Express **14**, 1996 (2006).
[8] M. Soljacic and J. D. Joannopoulos, Nature Mater. **3**, 211 (2004).
[9] M. Notomi, A. Shinya, S. Mitsugi, G. Kira, E. Kuramochi, and

T. Tanabe, Opt. Express **13**, 2678 (2005).
[10] T. Tanabe, M. Notomi, S. Mitsugi, A. Shinya, and E. Kuramochi, Opt. Lett. **30**, 2575 (2005).
[11] X. Yang, C. Husko, C. Wong, M. Yu, and D. Kwong, Appl. Phys. Lett. **91**, 051113 (2007).
[12] M. Notomi and S. Mitsugi, Phys. Rev. A **73**, 051803(R) (2006).
[13] M. Notomi, H. Taniyama, S. Mitsugi, and E. Kuramochi, Phys. Rev. Lett. **97**, 023903 (2006).
[14] T. Tanabe, M. Notomi, E. Kuramochi, A. Shinya, and H. Taniyama, Nat. Photonics **1**, 49 (2007).
[15] T. Tanabe, M. Notomi, S. Mitsugi, A. Shinya, and E. Kuramochi, Appl. Phys. Lett. **87**, 151112 (2005).
[16] T. Tanabe *et al.*, Appl. Phys. Lett. **90**, 031115 (2007).
[17] M. R. Singh, Phys. Lett. A **372**, 5083 (2008).
[18] Y. Ruan, K. Myung-Ki, Y.-H. Lee, B. Luther-Davies, and A. Rode, Appl. Phys. Lett. **90**, 071102 (2007).
[19] J. Aitchison, D. Hutchings, J. Kang, G. Stegeman, and A. Villeneuve, IEEE J. Quantum Electron. **33**, 341 (1997).
[20] A. Bristow, R. Iyer, J. Aitchison, H. van Driel, and A. Smirl, Appl. Phys. Lett. **90**, 101112 (2007).
[21] H. Oda, K. Inouse, Y. Tanaka, N. Ikeda, Y. Sugimoto, H. Ishikawa, and K. Asakawa, Appl. Phys. Lett. **90**, 231102 (2007).
[22] H. Oda, K. Inoue, A. Yamanaka, N. Ikeda, Y. Sugimoto, and K. Asakawa, Appl. Phys. Lett. **93**, 051114 (2008).
[23] F. Raineri, C. Cojocaru, P. Monnier, A. Levenson, R. Raj, X. Seassal, C. Letartre, and P. Viktorovitch, Appl. Phys. Lett. **85**, 1880 (2004).
[24] A. Yacomotti *et al.*, Appl. Phys. Lett. **88**, 231107 (2006).
[25] A. M. Yacomotti, P. Monnier, F. Raineri, B. B. Bakir, C. Seassal, R. Raj, and J. A. Levenson, Phys. Rev. Lett. **97**, 143904 (2006).
[26] H. Nakamura *et al.*, Opt. Express **12**, 6606 (2004).
[27] M. Dinu, F. Quochi, and H. Garcia, Appl. Phys. Lett. **82**, 2954 (2003).
[28] A. Bristow, J.-P. R. Wells, W. H. Fan, A. M. Fox, M. S. Skolnick, D. M. Whittaker, A. Tahraoui, T. F. Krauss, and J. S. Roberts, Appl. Phys. Lett. **83**, 851 (2003).
[29] C. Husko, A. D. Rossi, S. Combrié, Q. V. Tran, F. Raineri, and C. W. Wong, Appl. Phys. Lett. **94**, 021111 (2009).
[30] E. Weidner, S. Combriè, N. V. de Rossi, A. Quynh, S. Cassette, A. Talneau, and H. Benisty, Appl. Phys. Lett. **89**, 221104 (2006).
[31] E. Weidner, S. Combriè, A. de Rossi, N. V. Quynh, and S. Cassette, Appl. Phys. Lett. **90**, 101118 (2007).
[32] S. Combrié, N. V. Tran, D. Rossi, and H. Benisty, Opt. Lett. **33**, 1908 (2008).
[33] A. Shinya, S. Matsuo, Yosia, T. Tanabe, E. Kuramochi, T. Sato, T. Kakitsuka, and M. Notomi, Opt. Express **16**, 19382 (2008).
[34] C. P. Michael, K. Srinivasan, T. J. Johnson, O. Painter, K. H. Lee, K. Hennessy, H. Kim, and E. Hu, Appl. Phys. Lett. **90**, 051108 (2007).
[35] Y. Akahane, T. Asano, B. Song, and S. Noda, Nature (London) **425**, 944 (2003).
[36] S. Combrié, S. Bansropun, M. Lecomte, O. Parillaud, S. Cassette, H. Benisty, and J. Nagle, J. Vac. Sci. Technol. B **23**, 1521 (2005).
[37] S. Combrié, E. Weidner, A. De Rossi, S. Bansropun, S. Cassette, A. Talneau, and H. Benisty, Opt. Express **14**, 7353 (2006).
[38] M. Bass, *Handbook of Optics* (McGraw-Hill, New York, 1995).
[39] F. K. Reinhart, J. Appl. Phys. **97**, 123536 (2005).
[40] T. Carmon, L. Yang, and K. J. Vahala, Opt. Express **12**, 4742 (2004).
[41] P. E. Barclay, K. Srinivasan, and O. Painter, Opt. Express **13**, 801 (2005).
[42] T. Uesugi, B.-S. Song, T. Asano, and S. Noda, Opt. Express **14**, 377 (2006).
[43] X. Yang and C.-W. Wong, Opt. Express **15**, 4763 (2007).
[44] The *L3* cavity considered here is single mode over a large spectral range.
[45] H. Kawashima, Y. Tanaka, N. Ikeda, Y. Sugimoto, T. Hasama, and H. Ishikawa, IEEE J. Quantum Electron. **44**, 841 (2008).
[46] T. Tanabe, H. Taniyama, and M. Notomi, J. Lightwave Technol. **26**, 1396 (2008).
[47] Y. Yosia, A. Shinya, T. Tanabe, M. Notomi, and L. Chao, *Lasers and Electro-Optics* (CLEO/QELS, San Jose, CA, 2008); *Conference on Quantum Electronics and Laser Science, 2008* (CLEO/QELS, San Jose, CA, 2008), pp. 1–2.